




## Three-dimensional soliton-like distortions in flexoelectric nematic liquid crystals: modelling and linear analysis

Ashley Earls & M. Carme Calderer


To cite this article: Ashley Earls & M. Carme Calderer (2022) Three-dimensional soliton-like distortions in flexoelectric nematic liquid crystals: modelling and linear analysis, *Liquid Crystals*, 49:5, 742-757, DOI: [10.1080/02678292.2021.2006812](https://doi.org/10.1080/02678292.2021.2006812)

To link to this article: <https://doi.org/10.1080/02678292.2021.2006812>

 View supplementary material [↗](#)

 Published online: 11 Jan 2022.

 Submit your article to this journal [↗](#)

 Article views: 115

 View related articles [↗](#)

 View Crossmark data [↗](#)



# Three-dimensional soliton-like distortions in flexoelectric nematic liquid crystals: modelling and linear analysis

Ashley Earls<sup>a</sup> and M. Carme Calderer<sup>b</sup>

<sup>a</sup>Basque Center for Applied Mathematics (BCAM), Basic Center for Applied Mathematics, Bilbao, Spain; <sup>b</sup>School of Mathematics, University of Minnesota, Minneapolis, MN, USA

## ABSTRACT

This article models experimentally observed three-dimensional particle-like waves that develop in nematic liquid crystals, with negative dielectric and conductive anisotropy, when subject to an applied alternating electric field. The liquid crystal is confined in a thin region between two plates, perpendicular to the applied field. The horizontal, uniformly aligned director field is at equilibrium due to the negative anisotropy of the media. However, such a state is unstable to perturbations that manifest themselves as confined, bullet-like, director distortions travelling up and down the sample at a speed of several hundred microns per second. It is experimentally predicted that flexoelectricity plays a key role in generating the soliton-like behaviour. We develop a variational model that accounts for anisotropic dielectric, conductive, flexoelectric, elastic and viscous forces. We perform a stability analysis of the uniformly aligned equilibrium state to determine the threshold wave numbers, size, phase-shift and speed of the soliton-like disturbance. We show that the model predictions are in very good agreement with the experimentally measured values. The work models and analyzes a three-dimensional soliton-like instability reported, for the first time in flexoelectric liquid crystals, pointing towards a potential application as a new type of nanotransport device.

## ARTICLE HISTORY

Received 27 October 2021  
Accepted 11 November 2021

## KEYWORDS

Negative dielectric and conducting anisotropy; soliton-like wave; flexoelectricity; instability

## 1. Introduction

In this paper, we study a new type of three-dimensional soliton-like director field distortion observed in a flexoelectric nematic liquid crystals with negative dielectric anisotropy, subject to an (AC) alternating electric field [1]. The travelling disturbances, referred to as *director bullets*, *tuxedos* and *soliton-like* structures, consist of concentrated three-dimensional pattern of chevron-like distortion of molecular alignment of the liquid crystal propagating through a uniformly oriented sample. They arise as perturbations of the director field from the uniform state. Within the bullet region, the bow-like director perturbation oscillates with the frequency of the applied AC electric field and breaks the fore-aft symmetry, resulting in rapid propagation perpendicularly to the initial direction of alignment. They do not spread while moving over macroscopic distances a thousand times longer than their size. In this article, we build a mathematical model of the phenomenon that accounts for the intertwined effects of negative dielectric and electric charge conducting anisotropy together with the flexoelectric, bending

and viscous, contributions, all finely tuned, as collectively respond to the applied AC-field. We analyse the instability threshold of the undisturbed, uniformly aligned base solution and show that it characterises the size and speed of the emerging soliton-like disturbance. The governing system couples the Ericksen-Leslie equations of the dynamics of the director field  $\mathbf{n}$ , including dielectric and flexoelectric effects, but neglecting defects and flow, coupled with the Poisson-Nearst-Planck system of electric charge motion.

This paper models the experiments reported in [1], where a sample of 4 prime-butyl-4-heptyl-bicyclohexyl-4-carbonitrile (CCN-47) with impurities is confined between two parallel plates, located at  $z = 0$  and  $z = d$ , respectively, of a Cartesian coordinate system  $(x, y, z)$  of the Euclidian space. The plates form a cell of thickness  $d = 3 - 30$  (Figure 1, left picture). Initially, the director is uniformly aligned parallel to the plates,  $\mathbf{n}_0 = \hat{\mathbf{x}}$ , and an alternating electric field is then applied across the cell in the perpendicular direction to the plates,  $\mathbf{E}_0 = E_0 \cos \omega t \hat{\mathbf{z}}$ . Note that  $\mathbf{n}_0$  is an equilibrium state of the system due to the negative dielectric anisotropy of the media, with the property that molecules

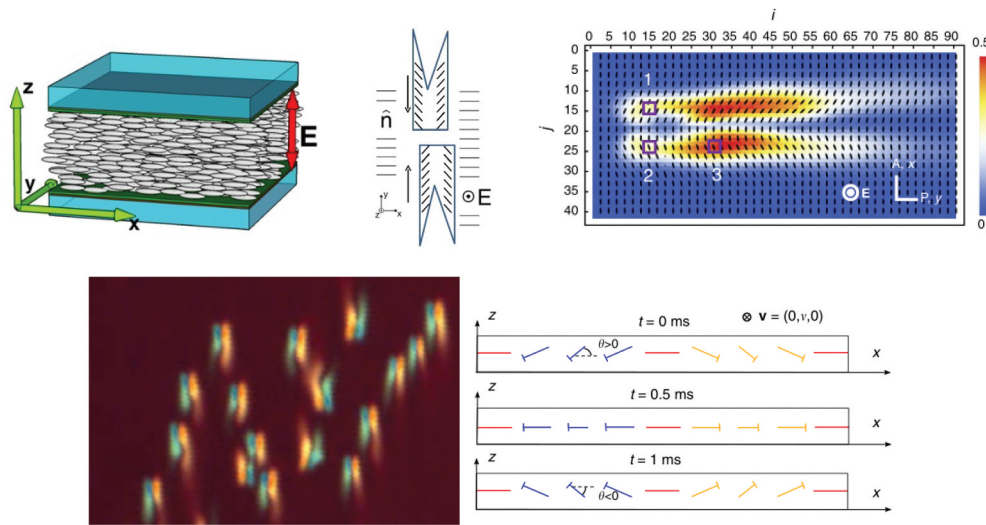


**Figure 1.** Top left: Geometry and initial alignment of the director field

tend to align on a plane perpendicular to the applied electric field. The amplitude of the applied voltage is within the range  $U = 10 - 90$ . Although a wide range of frequencies is being used in the experiment,  $\omega = 20 - 5000\text{Hz}$ , only the smaller interval between 400 and 460Hz is reported to generate soliton-like disturbance. Once generated, they travel up and down the region on the direction, taken to be the  $y$ -coordinate axis, perpendicular to both  $\mathbf{n}_0$  and  $\mathbf{E}_0$ . The bullets exhibit all the hallmarks of soliton behaviour: (1) they move with constant speed, (2) do not decay or disperse, and (3) retain their shape after pairwise collisions. Moreover, the disturbances form only in the middle plane of the cell,  $z = d/2$ , away from the bounding plates, and therefore are truly three-dimensional. Neither defects nor net flow are observed in the sample. To describe their shape, let us consider a single chevron and take the  $x$ -axis to be along its centre. The orthonormal set of unit vectors  $(\mathbf{n}, \mathbf{p}, \mathbf{m})$  play a main role in setting the geometry of the soliton-like package:

$$\begin{aligned} \mathbf{n} &= (\cos \theta \cos \phi, \cos \theta \sin \phi, \sin \theta), \\ \mathbf{m} &= (\sin \phi, -\cos \phi), \quad \mathbf{p} = \mathbf{n} \times \mathbf{m} \end{aligned} \quad (1)$$

with  $\mathbf{n}$  representing the parametrisation of the director field in terms of the angles  $\theta$ , out-of-plane, and  $\phi$ , the in- $(x,y)$  plane angle giving the disturbance a chevron form.

We develop a variational model that accounts for dielectric, conductive, flexoelectric, elastic and anisotropic viscous forces. It consists of a nonlinear parabolic system of partial differential equations for the dynamics of the director field  $\mathbf{n}$  and the Poisson-Nernst-Planck system for the diffusion and transport of electric charge, with  $c^+$  and  $c^-$  representing the concentrations of positive and negative ions, respectively. These equations are

coupled with Poisson's equation for the electrostatic potential  $\Phi$ . The equations of the director dynamics follow from the Ericksen-Leslie equations of liquid crystal flow setting the velocity field equal to zero, according to the experimental observation of no net flow taking place. The dimensional analysis of the governing equations reveals four time scales, that listed in increasing order include: the time scale of the dielectric effects  $T_d$ , the flexoelectric time scale  $T_f$  that is comparable in magnitude to that of the applied AC field  $T_\omega$  and finally that of the elastic effects,  $T_e$ . Furthermore, the time scale  $T_d$  is associated with the initial layer behaviour of the dielectric terms, acting at the beginning of every AC-cycle, approximately during the first 0.01 dimensionless time units. This allows us to obtain an approximate governing system, past the initial time, that excludes the appropriate dielectric terms. We also show that solutions of the governing system have the experimentally observed symmetry properties, and with every bullet travelling down along the  $y$ -axis, there is a symmetric one moving on the opposite direction. The predictions of the  $\frac{\pi}{2}$  phase-shift of the out-of-plane angle  $\theta$  is accurate within  $10^{-2}$  error.

Our work focuses on characterising the instability threshold of the uniform solution,  $\mathbf{n}_0$ , and explore the corresponding conditions to determine the size range, phase and speed of the subsequent disturbance. For this, we linearise the governing system about the basic state  $\mathbf{n}_0$  and take the double space Fourier transform of the resulting equations. The latter consists of a coupled system of three ordinary differential equations, with respect to the time variable  $t$ , for the angles  $\phi$  and  $\theta$  and the net charge  $q$  (the equation for the total charge,  $Q$ , decouples from the rest). The equations contain the

parameters of the problem together with the (justified as purely imaginary) wave numbers,  $\rho_x$  and  $\rho_\xi$ , of the perturbation, horizontal and vertical, respectively, (The vertical wave number refers to the travelling wave variable,  $\xi := y - Rt$ ,  $R$  being the dimensionless speed of the perturbation). We perform two main types of simplification on the system, first, we average it with respect to the cross-sectional variable  $z$ , with an ansatz motivated by a polynomial expansion of the unknown fields with respect to  $z$ , that captures the boundary conditions on top and bottom plates. The second simplifying assumption consists on a time averaging of the system with respect to the small parameter  $L_i^2$ , where  $L_i$  is a dimensionless constant measuring a relative strength of the flexoelectric effects (of the order  $O(10^{-3})$ ). Finally, the application of the variation of constants formula allows us to obtain the solution of the (approximated) governing system. We show that the uniform solution is an unstable node of the system, which together with the expressions of the general solutions allow us to formulate the conditions on the eigenvalues of the system that lead to (the approximate) neutral stability of the equilibrium state. These turn out to be, in part, conditions on the trace of two matrices, very much along the lines of the Floquet theory, leading to satisfactory bounds on the size of the disturbance. Specifically, the bound on the horizontal size, that of twice the distance between the two plates, is accurate, the vertical length of the disturbance as predicted by the model falls on the lower range of the experimentally measured soliton-like lengths, that is, between  $2.5 \times d$  and  $6.25 \times d \mu\text{m}$ , where  $d = 8\mu$ . The model underestimates the speed of the observed disturbance, by about a factor of  $\frac{1}{2}$ , also with respect to the lower bound values of experimental measurements. The linearity of the model may be responsible for the underpredictions. Our analysis also shows that, instabilities do not occur without flexoelectric polarisation in the model, and neither occur in the absence of ions [2]. Moreover, we find that the presence of ionic impurities as well as the increase of the absolute value of the anisotropic conductivity, each contributes to increasing the speed of the bullets. The shape of the chevron bullet is described in Figure 1. [34]. Middle sketch: schematic of the tuxedo structure and snapshot of tuxedo moving left in relation to the page [34] (top right). The direction field shows the angle  $\phi$  and the colour is the measured light intensity. The units are 1 along each axis. The planar angle  $\phi$  is largest at location 3, and  $\theta$  is zero in the chevron except at locations 1 and 2 [1]. Bottom left: tuxedos travelling up and down in relation to the page [34]. This is a top-down view of the middle plane between

the two plates, at  $z = 0$ . Bottom right: A schematic illustrating the angle  $\theta$  when the period of the external electric field is 2. The nails indicate the director  $\mathbf{n}$ , with the heads closer to the reader than the ends. The vector  $\mathbf{v}$  indicates the velocity of the chevron [1].

The pattern formation by application of an electric field to a liquid crystal has a long experimental and modelling history [3,4]. These patterns can be widely classified into two types, director distortions associated with the Freedericks transition [5,6] and electroconvective, along the vein of well-known phenomena, such as the Taylor-Bénard convection [7–9]. They are rooted in two key properties, the dielectric and conductive anisotropies,  $\varepsilon_a$  and  $\sigma_a$ , respectively, in addition to the geometry, either planar or homeotropic, of the undistorted director alignment  $n_0$ . We recall that in materials with  $\varepsilon_a > 0$ , the liquid crystal tends to align with the electric field, whereas the alignment is transverse in the negative case. Likewise, ionic impurities will move along the direction of the field for liquid crystals with  $\sigma_a > 0$ , and transversely otherwise.

Since the pioneering works by Williams [10] and Kaspustin and Larinova [11], there have been extensive experimental and theoretical investigations of the electro-hydrodynamic convection in nematic liquid crystals. In William's experiment, the nematic, characterised by  $\varepsilon_a < 0$  and  $\sigma_a > 0$ , is enclosed between two parallel plates, with separation  $d$  between 10 and 100  $\mu$ , in a geometry identical to the one in this work, with director alignment  $\mathbf{n}_0 = \hat{\mathbf{x}}$  (Figure 1, top left). Applying a low-frequency AC field, with a threshold maximum voltage of 10 V, convection rolls appear with associated director distortions, easily detected optically. These are rolls along the  $y$ -direction parallelly stacked next to each other, at a distance  $d$ , along the  $x$ -axis. Carr [12], provided the theoretical bases of the Williams domains, starting with the observation that the motion of ions along the electric field direction causes  $\mathbf{n}$  to tilt towards the  $z$  axis. Elastic forces resist the tilting, leading to a periodic equilibrium configuration with spatial concentrations of charge, especially in regions where the director gradient is large. Finally, the localised charge coupled with the electric field induces a circular flow reminiscent of Rayleigh-Bénard convection, with the same periodicity as the director field. This pattern persists even when the electric field changes sign, and as shown in [13], the critical voltage at which the Williams domains occur is independent of the sample thickness  $d$ . The first theoretical study of the Carr effect, in one-dimensional geometry, was carried out by Helfrich [14] followed by two-dimensional analyses of the phenomenon [15]. The full three-dimensional analysis as

well as the pattern formation for large frequencies (dielectric regime) and more general geometries was carried out by Kramer and Pesch [16]. Experiments and analysis of several liquid crystals revealed the three main features that characterise electroconvection: geometry (either planar or homeotropic alignment) and the signs of  $\varepsilon_a$  and  $\sigma_a$ . Liquid crystals such that  $\varepsilon_a\sigma_a < 0$  and, for both initial director field orientations, present primary convective pattern. However those such that  $\varepsilon_a < 0$  and  $\sigma_a < 0$ , with planar initial director orientation, fall into the class known as presenting non-standard Carr-Helfrich mechanism, with rarely observed convection phenomenon; they are still the subject of active investigation [17–19]. This is the case of the material in our study, and for which electroconvective phenomena has not been observed.

A related effect that does not involve ionic impurities comes from the often neglected flexoelectric polarisation, that is, the development of electric dipoles associated with director field gradients [20]. Each rod-shaped molecule of the nematic carries a small dipole moment, and in a nearly uniformly aligned sample, these dipoles nearly cancel and therefore have little effect. However, when the sample is subject to splay or bend type distortions, the small charges present on each molecule accumulate, leading to a spatial separation of charge. Flexoelectricity is also known to generate rich equilibrium spatial pattern [21]. Whereas Williams domains are entirely explained by ionic charge, soliton-packages cannot occur without flexoelectric polarisation, as observed in [1].

Soliton-like waves are ubiquitous to many physical systems and have been extensively studied [22]. Mathematically, solitons refer to solutions of distinctive partial differential equations associated with a Hamiltonian system, that in spite of being of dispersive type, present the three wave-particle features previously described. Although solitons are regarded as stable solutions of the PDE due to the long-time persistence of the shape, the question of their stability, specially for PDEs with critical non-linearity, remains one of the most challenging open problems of mathematical physics [23]. Equations of this class include the KdV equation, the wave equation, and the linear and nonlinear Schrödinger equations. Optical solitons in liquid crystals, *nematicons*, forming in nonlinear optic regimes prevalent, for instance, in applications to fibre optics, are associated with solutions of the latter [24,25]. The type of phenomena studied in this article falls into the class of particle-like waves known as *physical solitons*. The goal of the experimental work is to design new mechanisms of particle nanotrasport.

The article is organised as follows. In section 2, we derive the governing equations, obtain the relevant non-dimensional parameter groups and time-scales, in particular, leading to the identification of the initial layer term. In section 3, we linearise the PDE system about the initial uniform state and apply Fourier analysis and asymptotic analysis to obtain a sufficient condition for instability. Concluding remarks are given in section 5. This work is part of the Ph.D. thesis dissertation by Ashley Earls [26].

## 2. A model

The goal of this section is to derive the set of governing equations appropriate to describe the soliton-like phenomenon that we aim at investigating. We assume that the liquid crystal occupies a domain  $\Omega \subset \mathbb{R}^3$  that will later take to be the parallelepiped region confined between the two electrodes. The proposed model involves the main physical ingredients of the phenomenon: dielectric and flexoelectric polarisation, elastic, viscous and ionic effects, and the role of the alternating electric field. It also takes into account two main simplifying assumptions, one of them being the absence of an explicit role of defects in the evolution of the chevron structures, which are interpreted as travelling distortions of the molecular alignment that do not generate net flow. This allows us to describe the state of alignment of the liquid crystal by the unit director field  $\mathbf{n}$ , and follow a modelling approach based on the Ericksen-Leslie equations, suppressing flow but including electrodynamic effects and flexoelectric polarisation. Furthermore, rather than stating the laws of balance of linear and angular momentum of the system, we follow the variational approach associated with the principle of minimum dissipation. For this, we proceed to writing the total energy and the rate of dissipation function of the system, for the set of generalised variables  $\mathbf{q}$  and generalised velocities  $\dot{\mathbf{q}}$ . In addition to the director  $\mathbf{n}$ ,  $\mathbf{q}$  includes the family of charge concentration variables  $c^k$ ,  $1 \leq k \leq N$ , corresponding to  $N$  ionic species with valence  $z^k$ , and the electrostatic potential  $\Phi$ . The generalised velocities consist of  $\dot{\mathbf{n}}$ ,  $\dot{\Phi}$  and  $\mathbf{u}^k$ ,  $1 \leq k \leq N$ , the latter denoting the ionic velocity of the  $k$ th species. Let  $c_0 > 0$  denote a typical value of the concentration of one of the ionic families in the problem. The value of  $c_0$  specified in the table is that given in [1]. Approaches to precise measurements of such

a quantity in liquid crystal cells have been recently reported in the literature [27]. The ion concentrations satisfy the continuity equations

$$\frac{\partial c^k}{\partial t} + \mathbf{v} \cdot (c^k \mathbf{u}^k) = 0, \quad 1 \leq k \leq N. \quad (2)$$

The anisotropy of the liquid crystal is encoded in its dielectric tensor

$$\boldsymbol{\varepsilon}(\mathbf{n}) = \varepsilon_0(\varepsilon_{\perp} I + \varepsilon_a \mathbf{n} \otimes \mathbf{n}), \quad \varepsilon_a := \varepsilon_{\parallel} - \varepsilon_{\perp}, \quad (3)$$

where  $\varepsilon_0$  is the vacuum dielectric constant and  $\varepsilon_a$  denotes the dielectric anisotropy, the difference between the material-dependent parallel and perpendicular anisotropy coefficients. Flexoelectric materials are characterised by the electric displacement vector field

$$\mathbf{D}_{\text{elec}} = \boldsymbol{\varepsilon}(\mathbf{n})\mathbf{E} + \mathbf{P}_{\text{flex}}, \quad (4)$$

where  $\mathbf{P}_{\text{flex}}$  denotes the polarisation field of the material, that is, the dipolar density due to splay and bend distortions of the director field [4],

$$\begin{aligned} \mathbf{P}_{\text{flex}} &= e_1(\mathbf{v} \cdot \mathbf{n})\mathbf{n} + e_3(\mathbf{v} \times \mathbf{n}) \times \mathbf{n} \\ &= e_1(\mathbf{v} \cdot \mathbf{n})\mathbf{n} + e_3(\mathbf{n} \times \mathbf{v}). \end{aligned} \quad (5)$$

The coefficients  $e_1$  and  $e_3$  in (5) can be positive or negative, and the second equality in (5) follows from the identity  $\mathbf{v} \times (\mathbf{n} \times \mathbf{v}) = -(\mathbf{v} \cdot \mathbf{n})\mathbf{v}$  for  $|\mathbf{v}| = 1$ . The total energy density of the system consists of the contributions

$$\mathcal{E} = \mathcal{E}_{\text{OF}} + \mathcal{E}_{\text{dielc}} + \mathcal{E}_{\text{ion}} + \mathcal{E}_{\text{flex}} =: \tilde{\mathcal{E}} + \mathcal{E}_{\text{flex}}, \quad (6)$$

$\mathcal{E}_{\text{OF}}$  denoting the Oseen-Frank energy of director distortion, the dielectric electrostatic energy  $\mathcal{E}_{\text{dielc}}$ , the ionic contribution  $\mathcal{E}_{\text{ion}}$  which involves the entropy as well as the electrostatic energy of free charged particles, and the electrostatic contribution of the flexoelectric polarisation  $\mathcal{E}_{\text{flex}}$ . These are of the form

$$\begin{aligned} \mathcal{E}_{\text{OF}} &= \frac{1}{2}K_1(\mathbf{v} \cdot \mathbf{n})^2 + \frac{1}{2}K_2[\mathbf{n} \cdot (\mathbf{v} \times \mathbf{n})]^2 + \frac{1}{2}K_3|\mathbf{n} \times (\mathbf{v} \times \mathbf{n})|^2 \\ &\quad + \frac{1}{2}(K_2 - K_4)[\text{tr}^2(\mathbf{n} \otimes \mathbf{n}) - \text{tr}(\mathbf{n}^2)], \\ \mathcal{E}_{\text{dielc}} &= -\frac{1}{2}\varepsilon_0[|\mathbf{E}|^2 + \varepsilon_a(\mathbf{n} \cdot \mathbf{E})^2], \quad \mathcal{E}_{\text{ion}} = e\Phi \sum_{k=1}^N z^k c^k \\ &\quad + K_B T \sum_{k=1}^N c^k \ln\left(\frac{c^k}{c_0}\right), \quad \mathcal{E}_{\text{flex}} = -\mathbf{P}_{\text{flex}} \cdot \mathbf{E}, \end{aligned} \quad (7)$$

where the positive constants  $T$  and  $e$  denote the absolute temperature and the elementary charge, respectively, and  $K_B$  the Boltzman constant. The Frank elasticity constants  $K_i$  satisfy,  $K_1 > 0$ ,  $K_2 > 0$ ,  $K_3 > 0$ ,  $K_2 \geq |K_4|$ ,  $2K_1 \geq K_2 + K_4$ .

We briefly recall that the dynamics of a non-dissipative system, in a domain  $\Omega \subset \mathbb{R}^3$ , described by the generalised coordinates  $q_i$  and the generalised velocities  $\dot{q}_i$ , is given by the equations

$$X_i^e := \frac{d}{dt} \frac{\partial \mathcal{L}}{\partial \dot{q}_i} - \frac{\partial \mathcal{L}}{\partial q_i} = 0, \quad \mathcal{L} = \mathcal{T}(\dot{q}_i) - \mathcal{U}(q). \quad (8)$$

Here  $\mathcal{L}$  denotes the Lagrangian of the system, that is, the difference of the density of kinetic energy  $\mathcal{T}(\dot{q}_i)$ , the density of potential energy  $\mathcal{U}(q_i)$ , and  $X_i^e$  represents the elastic force [28]. The variational statement of this equation is  $\frac{\delta}{\delta \dot{q}_i} \int_{\mathcal{P}} \dot{\mathcal{E}} d\mathbf{x} = 0$ , where  $\mathcal{E} = \mathcal{L} + 2\mathcal{U}$  is the total energy of the system and  $\mathcal{P} \subseteq \Omega$ . That is, the system behaves in such a way that the rate of work is minimised with respect to the generalised velocities. Letting  $\mathcal{R} = \mathcal{R}(q_i, \dot{q}_i)$  represent the Rayleigh dissipation function, the dissipative forces are given by  $X_i^d = -\partial \mathcal{R} / \partial \dot{q}_i$ . The dynamics of a dissipative system is then formulated as the balance of the conservative forces by the dissipative ones, that is, the statement

$$\frac{d}{dt} \frac{\partial \mathcal{L}}{\partial \dot{q}_i} - \frac{\partial \mathcal{L}}{\partial q_i} + \frac{\partial \mathcal{R}}{\partial \dot{q}_i} = 0. \quad (9)$$

As in the conservative case, the above equations also have a variational interpretation in that they are critical points of the Rayleighian functional with respect to  $\dot{\mathbf{q}}$ :

$$\frac{\delta}{\delta \dot{q}_i} \int_{\mathcal{P}} (\dot{\mathcal{E}} + \mathcal{R} - \chi \mathbf{n} \cdot \dot{\mathbf{n}}) d\mathbf{x} = 0, \quad (10)$$

with the variations performed while holding  $\mathbf{q}$  and the elastic forces  $X_i^e$  constant. The last term in the previous equation corresponds to imposing the unit director constraint  $|\mathbf{n}| = 1$ , with  $\chi$  denoting the Lagrange multiplier. The two sources of energy dissipation of the system are the rotational viscosity of the director field and the diffusion of the ionic particles,

$$\mathcal{R} = \frac{1}{2}\gamma_1 |\dot{\mathbf{n}}|^2 + \frac{K_B T}{2} \sum_{k=1}^N c^k \mathbf{u}^k \cdot \mathcal{D}^{-1} \mathbf{u}^k, \quad (11)$$

where  $\mathbf{u}^k$  denotes the velocity of the  $k$ th ionic species (with respect to the nematic fluid, at zero velocity) and  $\mathcal{D}$  the diffusion matrix, taken to be the same for all ion types. The principle of minimum dissipation (10) yields the relations

$$0 = \frac{\delta}{\delta \dot{\mathbf{n}}} \int_{\Omega} (\dot{\mathcal{E}} + \mathcal{R} - \chi \mathbf{n} \cdot \dot{\mathbf{n}})$$

$$= \int_{\Omega} \left[ \frac{\partial}{\partial \mathbf{n}} (\mathcal{E}_{\text{OF}} + \mathcal{E}_{\text{flex}}) - \cdot \left( \frac{\partial}{\partial \mathbf{n}} (\mathcal{E}_{\text{OF}} + \mathcal{E}_{\text{flex}}) \right) - \chi \mathbf{n} + \gamma_1 \dot{\mathbf{n}} - \varepsilon_0 \varepsilon_a (\mathbf{n} \cdot \mathbf{E}) \mathbf{E} \right], \quad (12)$$

$$0 = \frac{\delta}{\delta \Phi} \int_{\Omega} \left( \tilde{\mathcal{E}} + \mathcal{R} - \chi \mathbf{n} \cdot \dot{\mathbf{n}} \right) = \int_{\Omega} \left[ - \cdot [\varepsilon_0 (\varepsilon_{\perp} \mathbf{I} + \varepsilon_a \mathbf{n} \otimes \mathbf{n}) \mathbf{E}] + e \sum_{k=1}^c N^k z^k - \cdot \mathbf{P}_{\text{flex}} \right], \quad (13)$$

$$0 = \frac{\delta}{\delta \mathbf{u}^k} \int_{\Omega} \left( \tilde{\mathcal{E}} + \mathcal{R} - \chi \mathbf{n} \cdot \dot{\mathbf{n}} \right) = \int_{\Omega} c^k \left[ \mu^k + K_B T \mathcal{D}^{-1} \mathbf{u}^k \right]. \quad (14)$$

These equations are complemented by the natural boundary conditions. The term  $\mu^k$  in (14) denotes the chemical potential associated with ion species  $k$ , given by

$$\mu^k = \frac{\partial \mathcal{E}_{\text{ion}}}{\partial c^k} = e \Phi z^k + K_B T \left[ \ln \left( \frac{c^k}{c_0} \right) + 1 \right], \quad 1 \leq k \leq N. \quad (15)$$

Therefore (14) yields  $\mathbf{u}^k = -\frac{1}{K_B T} \mathcal{D} \mu^k = -\mathcal{D} \left( \frac{c^k}{c^k} - \frac{e z^k}{K_B T} \mathbf{E} \right)$ . Substituting the latter into (2) and assuming that (12) and (13) hold for every subpart  $\mathcal{P} \subseteq \Omega$ , we arrive at the governing system of partial differential equations and the constraint relations:

$$\begin{cases} \frac{\partial \mathcal{E}_{\text{OF}}}{\partial \mathbf{n}} - \text{div} \left( \frac{\partial \mathcal{E}_{\text{OF}}}{\partial \mathbf{n}} \right) - \chi \mathbf{n} + \gamma_1 \dot{\mathbf{n}} - \varepsilon_0 \varepsilon_a (\mathbf{n} \cdot \mathbf{E}) \mathbf{E} \\ + (\varepsilon_3 - \varepsilon_1) [(\cdot \mathbf{n}) \mathbf{E} - \mathbf{n}^T \mathbf{E}] + (e_1 + e_3) (\mathbf{E} \mathbf{n}) \mathbf{n} = \mathbf{0}, \\ \cdot [\varepsilon_0 \varepsilon_{\perp} \mathbf{E} + \varepsilon_0 \varepsilon_a (\mathbf{n} \cdot \mathbf{E}) \mathbf{n} + e_1 (\cdot \mathbf{n}) \mathbf{n} + e_3 (\mathbf{n} \mathbf{n})] = e \sum_{k=1}^N z^k c^k, \\ \frac{\partial c^k}{\partial t} + \cdot \left[ \mathcal{D} \left( \frac{e z^k c^k}{K_B T} \mathbf{E} - c^k \right) \right] = 0, \\ \mathbf{n} \cdot \mathbf{n} = 1, \quad \mathbf{E} = - \Phi, \quad \Phi \text{ denotes the electrostatic potential.} \end{cases} \quad (16)$$

## 2.1. The governing equations of the chevron system

The experimental domain is the liquid crystal region  $\Omega$  enclosed between two parallel plates

$$\Omega = \left\{ (x, y, z) \in \mathbb{R}^3 : -\frac{L}{2} < x < \frac{L}{2}, 0 < y < L, 0 < x_3 < d \right\} = \Omega_{\perp} \times (0, d). \quad (17)$$

To describe the chevrons reported in [1], we make the following assumptions:

- (1) The simplifying, one-constant approximation of the Oseen-Frank energy, with  $K_1 = K_2 = K_3 = K$  and  $K_4 = 0$ .

- (2) There are two ion species present in the sample ( $N = 2$ ), with concentrations  $c^{\pm}$  and valences  $z^{\pm} = \pm 1$ .

- (3) The dielectric anisotropy is negative:  $\varepsilon_a < 0$ .

- (4) The diffusion matrix for the ions is given by

$$\mathcal{D} = \bar{D} [\mathbf{I} + (\lambda_{\sigma} - 1) \mathbf{n} \otimes \mathbf{n}], \quad \bar{D} = \frac{K_B T \sigma_{\perp}}{e^2 c_0}. \quad (18)$$

- (5) The conductive anisotropies satisfy  $\sigma_{\parallel} < \sigma_{\perp}$ , so  $\lambda_{\sigma} := \sigma_{\parallel} / \sigma_{\perp} < 1$ .

Using the Euler representations (1) of the unit vectors  $\{\mathbf{n}, \mathbf{m}, \mathbf{p}\}$ , the governing equations (16) become

$$\begin{cases} \gamma_1 \phi_t = K(\Delta \phi - 2 \tan \theta \phi \cdot \theta) + \varepsilon_0 \varepsilon_a [(\mathbf{n} \cdot \mathbf{E})(\mathbf{m} \cdot \mathbf{E}) \sec \theta + (e_1 + e_3) (\mathbf{E} \mathbf{n} \cdot \mathbf{m} \\ + (e_1 - e_3) [(\theta \cdot \mathbf{p})(\mathbf{E} \cdot \mathbf{m}) - (\theta \cdot \mathbf{m})(\mathbf{E} \cdot \mathbf{p})] \sec \theta], \\ \gamma_1 \theta_t = K(\Delta \theta + \frac{1}{2} \sin 2\theta |\phi|^2) + \varepsilon_0 \varepsilon_a [(\mathbf{n} \cdot \mathbf{E})(\mathbf{p} \cdot \mathbf{E}) + (e_1 + e_3) (\mathbf{E} \mathbf{n} \cdot \mathbf{p} \\ + (e_1 - e_3) \cos \theta [(\phi \cdot \mathbf{m})(\mathbf{E} \cdot \mathbf{p}) - (\phi \cdot \mathbf{p})(\mathbf{E} \cdot \mathbf{m})]], \\ \cdot [\varepsilon_0 \varepsilon_{\perp} \mathbf{E} - \varepsilon_0 \varepsilon_a (\mathbf{n} \cdot \mathbf{E}) \mathbf{n} + e_1 (\cdot \mathbf{n}) \mathbf{n} + e_3 (\mathbf{n} \mathbf{n})] = e(c^+ - c^-), \quad \mathbf{E} = - \Phi \\ c_t^{\pm} = \bar{D} \cdot [(\mathbf{I} + (\lambda_{\sigma} - 1) \mathbf{n} \otimes \mathbf{n}) (c^{\pm} \mp \frac{e z^{\pm}}{K_B T} \mathbf{E})]. \end{cases} \quad (19)$$

The unknown fields of the system are  $\phi$ ,  $\theta$ ,  $\Phi$ ,  $c^+$ , and  $c^-$ , with domain in  $\Omega$  and with  $t > 0$ . These equations form a coupled nonlinear parabolic-elliptic system with an electric field source term.

## 2.2. Scaling analysis and nondimensionalization

We define the dimensionless variables

$$\bar{x} = \frac{x}{L}, \quad \bar{y} = \frac{y}{L}, \quad \bar{z} = \frac{z}{d}, \quad \eta = \frac{d}{L}, \quad \bar{t} = \frac{t}{T}, \quad (20)$$

$$\bar{\Phi} = \frac{\Phi}{E_0 d}, \quad \bar{c}^{\pm} = \frac{c^{\pm}}{c_0},$$

where  $T > 0$  denotes a time scale to be chosen later and  $\eta > 0$  is the aspect ratio of the domain. Upon scaling, the domain  $\Omega$  and its cross-section  $\Omega_{\perp}$  in (17) become  $\bar{\Omega}$  and  $\bar{\Omega}_{\perp}$ , respectively. The scalar  $E_0 > 0$  denotes the maximum intensity of the applied AC field, with the product  $E_0 d$  representing the value of the electric potential applied to the system. Likewise,  $c_0 > 0$  denotes the typical concentration of a representative ionic species in the cell.

Parameter	Label	Value (SI)
Plate size	$L$	5
Plate separation	$d$	3 – 19.5
Frank elastic constant	$K$	$e - 11$
Rotational viscosity	$\gamma_1$	$6e - 2$
Temperature	$T$	313
Electric field intensity	$E_0$	$8.2e6$
Electric field frequency	$\omega$	400 – 450
Dielectric permittivity vacuum	$\varepsilon_0$	$8.85e - 12$
Dielectric anisotropy	$\varepsilon_a$	$-4.2$
Dielectric permittivity $\perp$	$\varepsilon_{\perp}$	$8.8$
Anisotropic conductivity $\parallel$	$\sigma_{\parallel}$	$4.9e - 9$
Anisotropic conductivity $\perp$	$\sigma_{\perp}$	$6.1e - 9$
Flexoelectric coefficients	$e_1, e_3$	on the order of $e - 11$
Typical charge concentration	$c_0$	$2e20$

The dimensionless version of the system (19) is

$$B\phi_t = C(\bar{\Delta}\phi - 2 \tan \theta \bar{\phi} \cdot \bar{\theta}) + (\mathbf{n} \cdot \bar{\mathbf{E}})(\mathbf{m} \cdot \bar{\mathbf{E}}) \sec \theta \\ + L_2 \sec \theta [\mathbf{m} \cdot (\bar{\mathbf{E}} \mathbf{n})] \\ + L_1 [(\bar{\theta} \cdot \mathbf{p})(\bar{\mathbf{E}} \cdot \mathbf{m}) - (\bar{\theta} \cdot \mathbf{m})(\bar{\mathbf{E}} \cdot \mathbf{p})] \sec \theta, \quad (21)$$

$$B\theta_t = C(\bar{\Delta}\theta + \frac{1}{2} \sin 2\theta |\bar{\phi}|^2) + (\mathbf{n} \cdot \bar{\mathbf{E}})(\bar{\mathbf{E}} \cdot \mathbf{p}) \\ + L_2 [\mathbf{p} \cdot (\bar{\mathbf{E}} \mathbf{n})] \\ + L_1 \cos \theta [(\bar{\phi} \cdot \mathbf{m})(\bar{\mathbf{E}} \cdot \mathbf{p}) - (\bar{\phi} \cdot \mathbf{p})(\bar{\mathbf{E}} \cdot \mathbf{m})], \quad (22)$$

$$\bar{\cdot} \cdot [J\bar{\mathbf{E}} - (\mathbf{n} \cdot \bar{\mathbf{E}})\mathbf{n} + (L_1 + L_2)(\bar{\cdot} \cdot \mathbf{n})\mathbf{n} + (L_1 - L_2)(\bar{\cdot} \cdot \mathbf{n})\mathbf{n}] \\ = M(c^+ - c^-), \\ \bar{\mathbf{E}} = -\bar{\Phi} \quad (23)$$

$$F c_t^\pm = \bar{\cdot} \cdot [(\mathbf{I} + (\lambda_\sigma - 1)\mathbf{n} \otimes \mathbf{n})(G^- c^\pm \mp c^\pm \bar{\mathbf{E}})]. \quad (24)$$

In (21)-(24), the rescaled differential operators are given by

$$\bar{\cdot} = \left( \eta \frac{\partial}{\partial \bar{x}}, \eta \frac{\partial}{\partial \bar{y}}, \frac{\partial}{\partial \bar{z}} \right), \quad \bar{\Delta} = \eta^2 \left( \frac{\partial^2}{\partial \bar{x}^2} + \frac{\partial^2}{\partial \bar{y}^2} \right) + \frac{\partial^2}{\partial \bar{z}^2}. \quad (25)$$

Table ?? summarises the parameters of the problem and their experimental values in [1].

The dimensionless coefficients are

$$B = \frac{\gamma_1 T^{-1}}{\epsilon_0 |\epsilon_a| E_0^2}, \quad C = \frac{K}{d^2 \epsilon_0 |\epsilon_a| E_0^2}, \quad L_1 = \frac{e_1 - e_3}{\epsilon_0 |\epsilon_a| E_0 d}, \quad L_2 = \frac{e_1 + e_3}{\epsilon_0 |\epsilon_a| E_0 d}, \\ J = \frac{\epsilon_1}{|\epsilon_a|}, \quad M = \frac{e c_0 d}{\epsilon_0 |\epsilon_a| E_0}, \quad F = \frac{K_B \Theta d T^{-1}}{e E_0 D} = \frac{e c_0 d}{E_0 \sigma_\perp}, \quad G = \frac{K_B \Theta}{e E_0 d}. \quad (26)$$

Observe that  $J > 1$  is always satisfied, guaranteeing the ellipticity of equation (23) with respect to  $\bar{\Phi}$ . Taking  $d = 8 \mu\text{m}$ , postponing the choice of  $T$ , and using the remaining values in table 2.2, we have

$$B = (2.4 \times 10^{-5} \text{s}) T^{-1}, \quad C = 6.25 \times 10^{-5}, \quad J = 2.1, \quad M = .84, \\ F = (5.1 \times 10^{-3} \text{s}) T^{-1}, \quad G = 4.1 \times 10^{-4}, \quad \lambda_\sigma = 0.8, \quad \eta = 1.6 \times 10^{-3}. \quad (27)$$

The flexoelectric constants  $e_1$  and  $e_3$  are difficult to measure experimentally, but they are on the order of  $10^{-11} \text{C m}^{-1}$  [29,30]. Therefore, the flexoelectric coefficients obey  $|L_1|, |L_2| \approx L_f$ , where

$$L_f := \frac{10^{-11} \text{C m}^{-1}}{\epsilon_0 \epsilon_a E_0 d} = 4.1 \times 10^{-3}. \quad (28)$$

Prior to choosing the value of  $T$  in the dimensionless parameter groups (27), we determine the time scales associated with the different effects of the model.

(1) Letting  $\omega$  be the frequency of the applied electric field, the corresponding time constant  $T_\omega = \frac{2\pi}{\omega}$  falls within the range

$$0.50\pi \times 10^{-2} \text{s} \geq T_\omega \geq 0.44\pi \times 10^{-2} \text{s}. \quad (29)$$

(2) The scale of dielectric effects follows from the relation  $B = 1$  and gives  $T_{\text{dielc}} = 0.21 \times 10^{-4} \text{s}$ .

(3) The scale of the flexoelectric effect follows from equating  $B = L_f$ , giving  $T_{\text{flex}} = 0.59 \times 10^{-2} \text{s}$ .

(4) The scale of the elastic effect follows from setting  $B = C$  and gives  $T_{\text{elast}} = 0.38 \text{s}$ .

The previous calculations indicate that, within the middle- to high-frequency range, the applied electric field activates the flexoelectric effects with a time scale of its own order of magnitude. This motivates us to choosing

$$T = 2\pi\omega^{-1}. \quad (30)$$

We also find that the dielectric effects relax faster, whereas the elastic ones evolve within a greater time scale. Typical values of the dimensionless constants, that will be taken as reference in the analysis, are calculated with  $\omega$  as in (29):

$$B = 1.2 \times 10^{-2}, \quad C = 6.3 \times 10^{-5}, \quad J = 2.1, \quad M = 0.84, \\ F = 2.6, \quad G = 4.1 \times 10^{-4}, \quad |L_1|, |L_2| \approx 4.1 \times 10^{-3}, \quad \lambda_\sigma = 0.8. \quad (31)$$

The scaled equations also reveal the dielectric effect as dominant and, with the flexoelectric one being between  $10^2$  and  $10^3$  times smaller. Moreover, for a sufficiently large electric field strength  $E_0$ ,  $|L_1|$  and  $|L_2|$  become very small, suppressing the flexoelectric mechanism. At such a limit, the appearance of convection would be expected. Next, we investigate the speed  $s$  of the soliton-like structure. In [1], the authors report speeds in the range of 150 to 400  $\mu$  m/sec. With the length of the electrode plate taken as 5.5 mm, the range of time scales  $T_s$  of the soliton motion is

$$T_{\text{min}}^s = \frac{5.5}{0.4} = 14 \text{s} \leq T_s \leq T_{\text{max}}^s = \frac{5.5}{0.1} = 55 \text{s}. \quad (32)$$

The dimensionless form of the soliton speed is taken as

$$R = \frac{s}{L\omega} = \frac{\eta s}{\omega d}. \quad (33)$$

Within the observed speed interval and the frequency range of the applied electric field, we find that

$$R_{\text{min}} = \frac{100}{5 \times 10^3 \times 450} = 0.444 \times 10^{-4} \leq R \leq R_{\text{max}} \\ = \frac{450}{5 \times 10^3 \times 400} = 2.25 \times 10^{-4}. \quad (34)$$



It remains to specify the initial and boundary conditions of the problem (21)–(24). These are

$$\begin{aligned} \theta(x, y, z, 0) &= \theta_0(\bar{x}, \bar{y}, \bar{z}), & \phi(x, y, z, 0) &= \phi_0(\bar{x}, \bar{y}, \bar{z}), \\ \bar{c}^\pm(x, y, z, 0) &= \bar{c}_0^\pm(\bar{x}, \bar{y}, \bar{z}). \end{aligned} \quad (35)$$

At  $\bar{x} = \pm \frac{1}{2}$ ,  $\bar{y} = 0, 1$ , and  $\bar{z} = 0, 1$ ,

$$\begin{aligned} \theta = \phi = 0, & & \bar{c}^+ - \bar{c}^- = 0, & & \bar{c}^+ + \bar{c}^- = Q_0 \\ \text{for all } \bar{t} \geq 0. \end{aligned} \quad (36)$$

Additionally,

$$\begin{aligned} \bar{\Phi}(\bar{x}, \bar{y}, 1, \bar{t}) &= \bar{\Phi}_0(\bar{t}), & \bar{\Phi}(\bar{x}, \bar{y}, 0, \bar{t}) &= 0, \\ \bar{x}, \bar{y} &\in \bar{\Omega}_\perp \end{aligned} \quad (37)$$

$$\bar{\Phi}_{\mathbf{n}}(\bar{x}, \bar{y}, \bar{z}, \bar{t}) = 0, \quad \bar{x}, \bar{y} \in \partial\bar{\Omega}_\perp, \quad 0 < \bar{z} < 1, \quad (38)$$

where  $\nu$  denotes the unit outer normal to the boundary  $\partial\bar{\Omega}_\perp$  (where corners are being excluded). The constant  $Q_0$  denotes a background charge concentration (both signs) representing the amount of impurities in the system. Assuming that there are two ion species in the sample, we take  $Q_0 = 2$ . Dirichlet boundary conditions on  $\mathbf{n}$  express the strong anchoring imposed on the bounding plates. Likewise, prescribing the electric potential on the plates is compatible with the waveform generator used in the experiment. For the charges, the assumption of Dirichlet boundary conditions instead of the standard no-flux is done for analysis convenience. Note that the initial profile of  $\bar{\Phi}$  can be computed from Poisson's equation and the conditions (35)–(38).

### 2.3. Travelling wave geometry, symmetry and time multiscale

We study travelling wave solutions that move along the  $y$ -axis with positive dimensionless speed  $R > 0$  as in (33). We therefore define the similarity variable

$$\bar{\xi} = \bar{y} - R\bar{t}, \quad (39)$$

However, for our current analysis, we treat  $R$  as one of the unknowns of the problem.

From this point forward, we suppress the superimposed bar notation on variables and look for solutions that depend on the variables  $t, x, z$ , and  $\xi$ . The partial derivatives transform as

$$\begin{aligned} \frac{\partial}{\partial y} &= \frac{\partial \xi}{\partial y} \frac{\partial}{\partial \xi} = \frac{\partial}{\partial \xi}, & \frac{d}{dt} &= \frac{\partial}{\partial t} + \frac{\partial \xi}{\partial t} \frac{\partial}{\partial \xi} = \frac{\partial}{\partial t} - R \frac{\partial}{\partial \xi}, \end{aligned} \quad (40)$$

and the corresponding gradient and Laplacian operators are

$$\boldsymbol{\varepsilon} = \left( \eta \frac{\partial}{\partial x}, \eta \frac{\partial}{\partial \xi}, \frac{\partial}{\partial z} \right), \quad \Delta_\xi = \eta^2 \left( \frac{\partial^2}{\partial x^2} + \frac{\partial^2}{\partial \xi^2} \right) + \frac{\partial^2}{\partial z^2}. \quad (41)$$

The governing system (21)–(24) becomes

$$\begin{cases} B\phi_t = BR\phi_\xi + C(\Delta_\xi \phi - 2 \tan \theta \boldsymbol{\varepsilon} \phi \cdot \boldsymbol{\varepsilon} \theta) + (\mathbf{n} \cdot \mathbf{E})(\mathbf{E} \cdot \mathbf{m}) \sec \theta + L_2[\mathbf{m} \cdot (\boldsymbol{\varepsilon} \mathbf{E})\mathbf{n}] \sec \theta \\ \quad - L_1(\boldsymbol{\varepsilon} \theta \cdot \mathbf{m})(\mathbf{E} \cdot \mathbf{p}) \sec \theta + L_1(\boldsymbol{\varepsilon} \theta \cdot \mathbf{p})(\mathbf{E} \cdot \mathbf{m}) \sec \theta, \\ B\theta_t = BR\theta_\xi + C(\Delta_\xi \theta + \frac{1}{2} \sin 2\theta |\boldsymbol{\varepsilon} \phi|^2) + (\mathbf{n} \cdot \mathbf{E})(\mathbf{E} \cdot \mathbf{p}) + L_2[\mathbf{p} \cdot (\boldsymbol{\varepsilon} \mathbf{E})\mathbf{n}] \\ \quad - L_1(\boldsymbol{\varepsilon} \phi \cdot \mathbf{p})(\mathbf{E} \cdot \mathbf{m}) \cos \theta + L_1 \cos \theta (\boldsymbol{\varepsilon} \phi \cdot \mathbf{m})(\mathbf{E} \cdot \mathbf{p}), \\ \boldsymbol{\varepsilon} \cdot [\mathbf{E} - (\mathbf{n} \cdot \mathbf{E})\mathbf{n} + \frac{1}{2}(L_1 + L_2)(\boldsymbol{\varepsilon} \cdot \mathbf{n})\mathbf{n} + \frac{1}{2}(L_2 - L_1)(\boldsymbol{\varepsilon} \cdot \mathbf{n})\mathbf{n}] = Mq, \\ FQ_t = FRQ_\xi + \boldsymbol{\varepsilon} \cdot [(\mathbf{I} + (\lambda_\sigma - 1)\mathbf{n} \otimes \mathbf{n})(G \boldsymbol{\varepsilon} Q - q\mathbf{E})], \\ Fq_t = FRq_\xi + \boldsymbol{\varepsilon} \cdot [(\mathbf{I} + (\lambda_\sigma - 1)\mathbf{n} \otimes \mathbf{n})(G \boldsymbol{\varepsilon} q - Q\mathbf{E})], \end{cases} \quad (42)$$

where the dimensionless variables

$$Q := c^+ + c^-, \quad q := c^+ - c^- \quad (43)$$

denote the total unsigned background charge and the net charge, respectively. The unknown dimensionless fields of the problem are  $\phi, \theta, \Phi, Q$ , and  $q$ .

We point out that choosing  $R > 0$  implies the selection of a disturbance moving in the positive  $y$ -direction. However, the experiments show that there are also chevrons moving in the opposite direction. Indeed, a simple calculation shows that, if there exists a chevron moving along the positive  $y$ -direction, there is a symmetric one moving opposite to it. We formulate this feature as follows:

#### 2.3.1. Symmetry property of the solutions

Suppose  $(\phi, \theta, \Phi, q)$  is a solution to (42) with speed  $R$ . Then

$$\begin{cases} \phi^*(x, \xi, t) = -\phi(x, -\xi, t), & \theta^*(x, \xi, t) = \theta(x, -\xi, t), \\ \Phi^*(x, \xi, t) = \Phi(x, -\xi, t), & \\ q^*(x, \xi, t) = q(x, -\xi, t), & Q^*(x, \xi, t) = Q(x, -\xi, t). \end{cases} \quad (44)$$

is a solution to (42) with speed  $-R$ . This property establishes that, for every soliton-like package moving with speed  $R$  along the positive direction, there is another one, with the opposite *bullet* profile (Figure 1, top-right illustration) that moves with the same speed along the negative direction.

#### 2.3.2. Initial layer property

We conclude this section observing that the governing system (42) has two main time scales, relevant to the dynamics of the angular profile  $\phi$  and  $\theta$ . These are the standard dimensionless time  $t$  and the *fast* time  $\hat{t} := \frac{t}{B}$ , with  $B$  as in (27). This motivates us to consider solutions of the system such that  $\theta = \theta(t, \hat{t}, x, \xi, z)$  and  $\phi = \phi(t, \hat{t}, x, \xi, z)$ . Furthermore, the size of the coefficients of the system, together with standard asymptotic arguments associated to initial layer analysis, allow us to approximate the angular equations of the governing system in the  $\hat{t}$  scale as

$$\begin{aligned} \phi_t &= (\mathbf{n} \cdot \mathbf{E})(\mathbf{E} \cdot \mathbf{m}) \sec \theta, & \theta_t &= (\mathbf{n} \cdot \mathbf{E})(\mathbf{E} \cdot \mathbf{p}), \\ \hat{t} &:= \frac{t}{B}. \end{aligned} \quad (45)$$

In particular, this indicates that, the initial conditions on the shape of the distortion that triggers the chevron are only felt at the very early time stages of the process, near  $t = 0$ , (lasting about  $10^{-2}$ , in dimensionless time). However, due to the periodicity of the source potential, the effect also reappears at  $t = n\pi$ ,  $n \geq 0$ , integer, where  $|p(n\pi)| = |\cos(n\pi)| = 1$ . This indicates that the dielectric effects, which depend only on the size of the applied field, are present in the system, discretely in time, manifesting themselves in a periodic fashion, with their action lasting about  $10^{-2}$  seconds. On the other hand, the soliton disturbance is almost entirely shaped by flexoelectric, viscous and elastic effects. We will revisit this property in reference to the linear system.

### 3. Instability of the uniform state

We take the point of view that soliton disturbances emerge at the instability onset of the uniform state. For this, we perform a stability analysis of such a state to determine the instability threshold, and the corresponding lengths and time scales associated with it. For this, we linearise the governing system (42) about the uniform state

$$\phi = \theta = 0, \quad \Phi = p(t)z, \quad q = 0, \quad Q = Q_0, \quad (46)$$

where

$$\mathbf{E} = -\Phi \quad \text{and} \quad p(t) = \cos t. \quad (47)$$

Note that the solution (46)-(47) satisfies the initial and boundary conditions (35)–(38) with  $\theta_0 = \phi_0 = 0$ ,  $c_0^\pm = \frac{1}{2}Q_0$ , and  $\Phi_0 = p(t)$ . This choice of  $\Phi$  corresponds to an alternating electric field in the  $z$ -direction, as in the experiments in [1]. Our goal is to show that this uniform solution is unstable to chevron-like travelling waves. For this, we proceed in several steps, that include approximating the original system as follows:

(1) Linearise the system about the equilibrium solution.

(2) Since the domain aspect ratio  $\eta$  is of the order of  $10^{-3}$ , we average the previously obtained system along the direction perpendicular to the plates.

(3) We take the Fourier transform of the resulting system with respect to the space variables  $x$  and  $\xi$ .

(4) We formulate the conditions on the combined parameters and Fourier modes that lead to neutral stability, and analyse the resulting relations.

The linear system, with respect to the time scale  $t$  is

$$\begin{cases} B\phi_t = BR\phi_\xi + C\bar{\Delta}_\xi\phi + L_1\eta p(t)\theta_\xi + L_2\eta^2\Phi_{x\xi}, \\ B\theta_t = BR\theta_\xi + C\bar{\Delta}_\xi\theta - p(t)\eta\Phi_x - L_1\eta p(t)\phi_\xi + L_2\eta^2\Phi_{xz}, \\ (J-1)\eta^2\Phi_{xx} + J\eta^2\Phi_{\xi\xi} + J\Phi_{zz} = p(t)\eta\theta_x + L_2\eta^2\phi_{x\xi} + \eta\theta_{xz} - Mq, \\ Fq_t = FRq_\xi + G(\lambda_\sigma\eta^2q_{xx} + \eta^2q_{\xi\xi} + q_{zz}) + p(t)Q_z \\ \quad + Q_0[\lambda_\sigma\eta^2\Phi_{xx} + \eta^2\Phi_{\xi\xi} + \Phi_{zz} + (\lambda_\sigma - 1)p(t)\eta\theta_x], \\ FQ_t = FRQ_\xi + G(\lambda_\sigma\eta^2Q_{xx} + \eta^2Q_{\xi\xi} + Q_{zz}) + p(t)q_z. \end{cases} \quad (48)$$

**Remark 1.** Observe that if the flexoelectric terms are removed ( $L_1 = L_2 = 0$ ), the equation for  $\phi$  is simply

$$B\phi_t = BR\phi_\xi + C\Delta_\xi\phi, \quad (49)$$

which is the heat equation with a lower-order terms. Without flexoelectricity, there is no forcing in the equation, and the  $\phi$  profile will dissipate to zero. However, the experiments show that the  $\phi$  profile is roughly constant in time. This provides strong evidence that the flexoelectricity is indeed responsible for the formation of the chevrons.

#### 3.1. Space averaging

The averaging performed next, while reducing the problem to the two-dimensional space variables  $x$  and  $\xi$  is consistent with the three-dimensional nature of the chevron [1]. In particular, it allows for the trivial boundary conditions on the angular and concentration variables to hold on the boundary plates  $z = 0$  and  $z = 1$ , and the electric field taking the prescribed values on the electrodes. This, in turn, is consistent with the observation that the director disruption occurs in a thin region around the middle of the domain. Motivated by the techniques of approximating functions by sums of orthogonal polynomials, we assume that the  $z$ -dependence of the fields follows the parabolic profile,

$$\begin{aligned} \phi &= r(z)\tilde{\phi}(x, \xi, t), & \theta &= r(z)\tilde{\theta}(x, \xi, t), & \Phi &= r(z)\tilde{\Phi}(x, \xi, t), \\ q &= r(z)\tilde{q}(x, \xi, t), & Q &= r(z)\tilde{Q}(x, \xi, t), \end{aligned} \quad (50)$$

where  $r(z) = 6z(1-z)$ . Then

$$\begin{aligned} f_0^1 r(z) dz &= 1, & f_0^1 r'(z) dz &= 0, \\ f_0^1 r''(z) dz &= -12, \end{aligned} \quad (51)$$

so after averaging in  $z$  (and dropping the tildes), the linear system (48) becomes

$$\begin{cases} B\phi_t = BR\phi_\xi + C(\eta^2\phi_{xx} + \eta^2\phi_{\xi\xi} - 12\phi) + L_1\eta p(t)\theta_\xi + L_2\eta^2\Phi_{x\xi}, \\ B\theta_t = BR\theta_\xi + C(\eta^2\theta_{xx} + \eta^2\theta_{\xi\xi} - 12\theta) - p^2(t)\theta - p(t)\eta\Phi_x - L_1\eta p(t)\phi_\xi, \\ (J-1)\eta^2\Phi_{xx} + J\eta^2\Phi_{\xi\xi} - 12J\Phi = p(t)\eta\theta_x + \eta^2L_2\phi_{x\xi} - Mq, \\ Fq_t = FRq_\xi + G(\lambda_\sigma\eta^2q_{xx} + \eta^2q_{\xi\xi} - 12q) + Q_0(\lambda_\sigma\eta^2\Phi_{xx} + \eta^2\Phi_{\xi\xi} - 12\Phi) \\ \quad + Q_0(\lambda_\sigma - 1)p(t)\eta\theta_x. \end{cases} \quad (52)$$

and

$$FQ_t = FRQ_\xi + G(\lambda_\sigma \eta^2 Q_{xx} + \eta^2 Q_{\xi\xi} - 12Q) \quad (53)$$

The equation (53) for  $Q$  decouples from the rest of the system, so it can be disregarded. The total concentration of ions enters (52) only through the constant  $Q_0$ .

### 3.2. Fourier analysis

We adopt the method of the Fourier transform to determine instability thresholds of the base solution (46)–(47). The perturbation functions are twice continuously differentiable and are also elements of  $L^1(\mathbb{R}^2)$ . This assumptions are consistent with two of the main aspects of the phenomenon: the triggering body force mechanism due to the applied electric field, rather than conditions at the boundary, and the persistence of the uniform base configuration away from the plane centre region. This justifies the trivial extension of the base solution to the entire  $x - \xi$  plane.

We start with applying the Fourier transform to (52) in both  $x$  and  $\xi$ , i.e.

$$\hat{f}(\rho_x, \rho_\xi) = \int_{\mathbb{R}^2} f(x, y) \exp(-2\pi i(\rho_x x + \rho_\xi \xi)) dx d\xi. \quad (54)$$

Poisson's equation gives

$$\hat{\Phi} = \frac{1}{4\Delta_J(\rho_x, \rho_\xi)} \left( 4\pi^2 \eta^2 L_2 \rho_x \rho_\xi \hat{\Phi} - 2\pi i \eta p(t) \rho_x \hat{\theta} + M \hat{q} \right) \quad (55)$$

with

$$\Delta_J(\rho_x, \rho_\xi) = (J - 1)\eta^2 \pi^2 \rho_x^2 + J\eta^2 \pi^2 \rho_\xi^2 + 3J. \quad (56)$$

In order to solve (55), we assume that  $\Delta_J(\rho_x, \rho_\xi) \neq 0$ . Substituting (55) into the remaining equations for  $\hat{\Phi}$ ,  $\hat{\theta}$  and  $\hat{q}$  in (52) yields

$$\begin{aligned} B\hat{\Phi}_t = & \left[ 2\pi i B R \rho_\xi - 4C\Delta_1(\rho_x, \rho_\xi) - \frac{4\pi^4 L_2^2 \eta^4 \rho_x^2 \rho_\xi^2}{\Delta_J(\rho_x, \rho_\xi)} \right] \hat{\Phi} \\ & + 2\pi i \eta \rho_\xi p(t) \left( L_1 + \frac{\pi^2 L_2 \eta^2 \rho_x^2}{\Delta_J(\rho_x, \rho_\xi)} \right) \hat{\theta} - \frac{\pi^2 L_2 M \eta^2 \rho_x \rho_\xi}{\Delta_J(\rho_x, \rho_\xi)} \hat{q}, \end{aligned} \quad (57)$$

$$\begin{aligned} B\hat{\theta}_t = & \left[ 2\pi i B R \rho_\xi - 4C\Delta_1(\rho_x, \rho_\xi) - \left( 1 + \frac{\pi^2 \eta^2 \rho_x^2}{\Delta_J(\rho_x, \rho_\xi)} \right) p^2(t) \right] \hat{\theta} \\ & - 2\pi i \eta \rho_\xi \left( L_1 + \frac{L_2 \pi^2 \eta^2 \rho_x^2}{\Delta_J(\rho_x, \rho_\xi)} \right) \hat{\Phi} p(t) - \frac{\pi i M \eta \rho_x}{2\Delta_J(\rho_x, \rho_\xi)} \hat{q} p(t) \end{aligned} \quad (58)$$

$$\begin{aligned} F\hat{q}_t = & \left( 2\pi i F R \rho_\xi - 4G\Delta_\sigma(\rho_x, \rho_\xi) - \frac{Q_0 M \Delta_\sigma(\rho_x, \rho_\xi)}{\Delta_J(\rho_x, \rho_\xi)} \right) \hat{q} \\ & - 4\pi^2 \eta^2 Q_0 L_2 \rho_x \rho_\xi \frac{\Delta_\sigma(\rho_x, \rho_\xi)}{\Delta_J(\rho_x, \rho_\xi)} \hat{\Phi} \\ & + 2\pi i \eta Q_0 \rho_x \left( \lambda_\sigma - 1 + \frac{\Delta_\sigma(\rho_x, \rho_\xi)}{\Delta_J(\rho_x, \rho_\xi)} \right) \hat{\theta} p(t), \end{aligned} \quad (59)$$

where

$$\begin{aligned} \Delta_\sigma(\rho_x, \rho_\xi) &= 3 + \pi^2 \eta^2 (\lambda_\sigma \rho_x^2 + \rho_\xi^2), \quad \Delta_1(\rho_x, \rho_\sigma) \\ &= 3 + \pi^2 \eta^2 (\rho_x^2 + \rho_\xi^2). \end{aligned} \quad (60)$$

Our goal is to identify neutrally stable solutions of the previous system that also allow for the sustained time oscillation of the out of plane angular variable  $\theta$ . Now, let us formally write the system as

$$\mathbf{u}_t = \mathbf{A}(t)\mathbf{u}, \quad \mathbf{u} = [\hat{\Phi} \quad \hat{\theta} \quad \hat{q}], \quad (61)$$

where  $\mathbf{A}$  is directly obtained from the coefficients of equations (57)–(59). Suppressing the dependence of  $\Delta_1$ ,  $\Delta_J$ , and  $\Delta_\sigma$  on  $\rho_x$  and  $\rho_\xi$ , we find that the components of the matrix  $\mathbf{A}$  are:

$$\begin{aligned} A_{11} &= V - a_{11}, \\ A_{12}(t) &= -A_{21}(t) \\ &= \frac{2\pi i \eta \rho_\xi}{B\Delta_J} [JL_1 \Delta_1 + \pi^2 \eta^2 (L_2 - L_1) \rho_x^2] p(t), \\ A_{13} &= -\frac{\pi^2 L_2 M \eta^2 \rho_x \rho_\xi}{B\Delta_J}, \quad A_{22}(t) = V - a_{22}(t), \\ A_{23} &= -\frac{\pi i M \rho_x \eta}{2B\Delta_J} p(t), \\ A_{31} &= -\frac{4\pi^2 \eta^2 Q_0 L_2 \rho_x \rho_\xi \Delta_\sigma}{F \Delta_J}, \\ A_{32}(t) &= \frac{2\pi i \lambda_\sigma Q_0 \eta \rho_x \Delta_1}{F \Delta_J} p(t), \quad A_{33} = V - a_{33}, \end{aligned} \quad (62)$$

where

$$V = 2\pi i R \rho_\xi, \quad a_{11} = \frac{4}{B} \left( C\Delta_1 + \frac{\pi^4 L_2^2 \eta^4 \rho_x^2 \rho_\xi^2}{\Delta_J} \right), \quad (63)$$

$$a_{22}(t) = \frac{4C}{B} \Delta_1 - \frac{J \Delta_1}{B \Delta_J} p^2(t) := \tilde{a}_{22} - \frac{J \Delta_1}{B \Delta_J} p^2(t),$$

$$a_{33} = \frac{\Delta_\sigma}{F} \left( 4G + \frac{Q_0 M}{\Delta_J} \right).$$

(64)

**Remark 2.** We point out that the second term in  $a_{22}(t)$  in (64) is of order  $O(1)$ , except for the special wave numbers on the line  $\Delta_1 = 0$ . Away from the latter case, the separation of time scales, between  $t$  and  $\frac{t}{B}$ , indicates that the  $p^2(t) -$  term contributes to the initial layer of the solution  $\theta$ , and as such, it should be treated separately from the time- $t$  dynamics, as customary in initial layer analyses [31]. Consequently, from now on, we will omit the  $p^2(t) -$  term from  $A_{22}$  and  $a_{22}$  and replace them with  $\tilde{A}_{22}$  and  $\tilde{a}_{22}$ , respectively.

In order to analyse the stability of the system (61)-(62), we restrict the wave number variables to purely imaginary, that is,

$$\operatorname{Re} \rho_x = \operatorname{Re} \rho_\xi = 0. \tag{65}$$

The condition (65) simplifies the calculations, but it also matches the experimental findings. Since the chevrons do not exhibit periodic behaviour in either the  $x$ - or  $y$ -directions, we expect the real parts of the Fourier variables  $\rho_x$  and  $\rho_\xi$  to be zero. Taking  $\rho_x$  and  $\rho_\xi$  purely imaginary means that solutions display exponential growth or decay in both the  $x$ - and  $y$ -directions. We note that, under the assumption (65), all the components of  $\mathbf{A}$  in (62) are real-valued. Let us introduce the notation

$$c_x = -\pi^2 \eta^2 \rho_x^2, \quad c_\xi = -\pi^2 \eta^2 \rho_\xi^2 \tag{66}$$

It follows from the condition (65) that  $c_x, c_\xi \geq 0$ . The choice of the sign of  $\operatorname{Im} \rho_\xi$  will be done later, when sorting out the sign of  $R$ .

**Proposition 3.1.** *Let us consider perturbations satisfying (65). Then, the equilibrium solution (46)-(47) of the problem (61), for parameter data as in (31), is unstable for perturbations whose speed and wave numbers satisfy*

$$\begin{aligned} & -6\pi R \operatorname{Im} \rho_\xi - H(c_x, c_\xi) \geq 0 \quad \text{and} \quad \Delta_J \neq 0, \\ H(c_x, c_\xi) & := \frac{1}{B\Delta_J} [8C\Delta_1\Delta_J + 4L_2^2 c_x c_\xi \Delta_J + \frac{1}{2}\Delta_1 + \frac{\Delta_0}{F} (4G + BQ_0M)], \end{aligned} \tag{67}$$

and, with  $c_x$  and  $c_\xi$  as in (66).

**Proof.** Let  $\mu_1, \mu_2$ , and  $\mu_3$  denote the Floquet exponents of the system [32]. Recall the trace property of the Floquet theory of linear systems with periodic coefficients, that is,

$$\sum_{i=1}^3 \mu_i = \int_0^1 \operatorname{tr} \mathbf{A}(t) dt, \tag{68}$$

$$\begin{aligned} \operatorname{tr}(\mathbf{A}) &= 6\pi i R \rho_\xi - \frac{8C\Delta_1(\rho_x, \rho_\xi)}{B} - \frac{4\pi^4 L_2^2 \eta^2 \rho_x^2 \rho_\xi^2 + Jp^2(t)}{B\Delta_J(\rho_x, \rho_\xi)} \\ &\quad - \frac{\Delta_\sigma(\rho_x, \rho_\xi)}{F} \left( 4G + \frac{Q_0M}{\Delta_J(\rho_x, \rho_\xi)} \right). \end{aligned} \tag{69}$$

The result follows by integrating (69) with respect to  $t$  and taking into account that the diagonal elements are all constant, except for the  $p^2(t)$  term appearing in the component  $A_{22}$  of (62), and then setting  $\int_0^1 \operatorname{tr} \mathbf{A}(t) dt \geq 0$ . The positivity of (67) ensures that at least one Floquet exponent has positive real part.  $\square$

**Remark 3.** Inequality (67) provides a useful insight in finding the threshold conditions that trigger the instability of the uniform solution. For this, we need to identify wave number parameters that satisfy the equation  $H(c_x, c_\xi) = 0$ , for perturbations with speed  $R = 0$ . In a later section, we will further interpret the wave number equation in terms of the eigenvalues of the system that characterise the neutral stability of the uniform solution.

We summarise the main results of this work on the following theorem. For this, we first rewrite the linear system (59) in the form

$$\dot{\mathbf{u}} = \mathbf{A}^0 \mathbf{u} + \mathbf{h}(t), \tag{70}$$

where

$$A_{ij}^0 = A_{ij}, \quad i = j = 1, 3; \quad A_{22}^0 = \tilde{A}_{22},$$

$$A_{13}^0 = A_{13}, \quad A_{23}^0 = A_{23}, \quad A_{31}^0 = A_{31}, \quad A_{12}^0 = 0, \quad A_{21}^0 = 0,$$

$$\mathbf{h} = [A_{12}(t)\hat{\theta} \quad A_{21}(t)\hat{\phi} \quad A_{32}(t)\hat{\theta}]^T, \tag{71}$$

**Theorem 3.2.** *Suppose that  $\epsilon_a < 0$  and  $\lambda_\sigma < 1$ , and that the parameters of the problem are as in (27). There exist wave numbers  $\rho_x, \rho_\xi$  and perturbation speeds  $R$ , for which  $\lambda_1 \geq \lambda_3 \geq 0$ , where  $\lambda_i, i = 1, 3$ , denote the eigenvalues of the matrix  $\mathbf{A}^0$ , so that the solution  $\mathbf{u} = [0 \quad 0 \quad 0]^T$  of the Fourier system (59) is an unstable node. Moreover, for the wave numbers and perturbation speeds satisfying the stricter relations (99),  $\lambda_1 \approx 0 \approx \lambda_3$  hold up to terms of the order  $O(10^{-5})$ . Furthermore, the perturbations that solve the approximate linear system obtained from equation (59) by time averaging of two appropriate off-diagonal terms have the property that the out-of plane angle  $\hat{\theta}$  has a nonzero phase-shift of approximately  $\frac{\pi}{2}$  radians with*

respect to the applied electric field. Moreover, the size of the unstable perturbations and the chevron speed fall within the experimental range.

**Remark 4.** The requirement that (99) hold ensures the vanishing of the eigenvalues  $\lambda_1$  and  $\lambda_3$ . Equivalently, it amounts to a selection of wave numbers and speeds of the perturbations in the neutral stability regime, that is, at the instability threshold, that preserve the shapes of the components  $\phi$  and  $q$ .

The proof is carried out in the next subsection, and it proceeds in four steps. For notational convenience, we will suppress the ‘hat’ symbol from the fields  $\phi, \theta, q$ .

### 3.3. Solution of the linear system

Next, we solve the system (61) with respect to the time variable  $t$ , with the wave numbers playing the role of parameters of the system. We further identify ranges of such parameters that lead to neutral stability of the solutions. Two approximations will enter the analysis, one involving time averaging of two off diagonal terms of the order  $O(L_i)$ . A second one, that replaces the positive term  $p^2(t)$ , on the main diagonal of the system, by its one-period average  $\frac{1}{2}$ , is done in order to replace an otherwise longer calculation.

**Step 1.** We start solving the homogeneous system (70). It corresponds to the three ordinary differential equations

$$\begin{bmatrix} \phi_t \\ q_t \end{bmatrix} = \begin{bmatrix} A_{11} & A_{13} \\ A_{31} & A_{33} \end{bmatrix} \begin{bmatrix} \phi \\ q \end{bmatrix}, \quad (72)$$

$$\theta_t = A_{22}^0 \theta + A_{23}(t)q. \quad (73)$$

The characteristic equation associated with the problem (72) is

$$\lambda^2 - \text{tr}(A^0)\lambda + \det A^0 = 0. \quad (74)$$

The roots are

$$\begin{aligned} \lambda_1 &= \frac{1}{2} [\text{tr}(A^0) + \sqrt{\text{tr}^2(A^0) - 4 \det A^0}], \\ \lambda_3 &= \frac{1}{2} [\text{tr}(A^0) - \sqrt{\text{tr}^2(A^0) - 4 \det A^0}]. \end{aligned} \quad (75)$$

Let us rewrite

$$\lambda_{1,3} = \frac{1}{2} [(A_{11} + A_{33}) \pm \sqrt{(A_{11} - A_{33})^2 + 4A_{13}A_{31}}]. \quad (76)$$

The corresponding eigenvectors are

$$\mathbf{v}_1 = \begin{bmatrix} \omega_1 \\ 1 \end{bmatrix}, \quad \mathbf{v}_3 = \begin{bmatrix} \omega_3 \\ 1 \end{bmatrix}, \quad (77)$$

where

$$\omega_1 := -\frac{A_{13}}{A_{11} - \lambda_1}, \quad \omega_3 := -\frac{A_{13}}{A_{11} - \lambda_3}, \quad \omega_1 \neq \omega_3. \quad (78)$$

The general solution to the system (72) is

$$\begin{bmatrix} \phi(t) \\ q(t) \end{bmatrix} = a_0 e^{\lambda_1 t} \mathbf{v}_1 + b_0 e^{\lambda_3 t} \mathbf{v}_3, \quad (79)$$

where  $a_0$  and  $b_0$  are arbitrary constants. Note that two relevant cases arise according to the nature of the eigenvalues  $\lambda_1, \lambda_3$ :

$$\begin{aligned} (i) &: \text{tr}^2(A^0) - 4 \det A^0 \geq 0, \quad \text{and} \\ (ii) &: \text{tr}^2(A^0) - 4 \det A^0 < 0. \end{aligned} \quad (80)$$

They correspond to the equilibrium solution  $[0, 0]^T$  of (72) being, (i) a node or saddle point, or (ii) a spiral. To help us determine the wave number ranges consistent with the soliton-like instability, we set up the following lemma.

**Lemma 3.3.** Assume that  $\text{tr} \mathbf{A}_0 \geq 0$ . Let us consider wave numbers such that ((65)) holds. Then for both cases (i) and (ii) in (80) the  $[0, 0]^T$  solution of (72) is unstable. Furthermore, for parameter values as in (31), the product

$$A_{13}A_{31} = \frac{L_2^2 M Q_0 \Delta_\sigma}{BF \Delta_\gamma^2} c_x c_\xi = 0 \Leftrightarrow \Delta_\sigma = 0. \quad (81)$$

Let us consider the wave number range such that

$$\lambda_1 \geq \lambda_3 \geq 0. \quad (82)$$

We will find that such a range is consistent with (81) being satisfied to the order  $O(L_i^2 \times 10^{-2})$ . In such a case,  $[0, 0]^T$  is an unstable node. Let us now consider the solution to (72) along the invariant line  $\mathbf{v}_1 = 0$ , and apply it to equation (73), that now takes the form

$$\theta_t = A_{22}^0 \theta + b_0 A_{23}(t) e^{\lambda_3 t}. \quad (83)$$

Note that departure from the branch  $\mathbf{v}_1$  eliminates the highest decay rate,  $\lambda_1$ , from the solution. The general solution of the latter equation is then

$$\Theta(t) = \exp\left(\int_0^t A_{22}^0(s) ds\right) (C_0 + X(t)), \quad (84)$$

$$X(t) := b_0 \int_0^t \exp\left[-\int_0^s A_{22}^0(u) du\right] A_{23}(s) e^{\lambda_3 s} ds, \quad (85)$$

where  $b_0$  and  $C_0$  are arbitrary constants. We also make the simplifying assumption of replacing  $A_{22}(t)$  by its average on the interval  $[0, 1]$ , and we arrive at

$$\begin{aligned} X(t) &= \int_0^t e^{(\lambda_3 - A_{22}^0)s} A_{23}(s) ds \\ &= \frac{M\sqrt{c_x}}{2B\Delta_J} \frac{e^{(\lambda_3 - A_{22}^0)t}}{(\lambda_3 - A_{22}^0)^2 + 4\pi^2} [2\pi \sin 2\pi t + (\lambda_3 - A_{22}^0) \cos 2\pi t]. \end{aligned}$$

Hence,

$$\begin{aligned} \Theta(t) &= C_0 e^{A_{22}^0 t} \\ &+ b_0 \frac{M\sqrt{c_x}}{2B\Delta_J} \frac{e^{\lambda_3 t}}{(\lambda_3 - A_{22}^0)^2 + 4\pi^2} [2\pi \sin 2\pi t \\ &+ (\lambda_3 - A_{22}^0) \cos 2\pi t]. \end{aligned} \quad (86)$$

We immediately observe the phase shift of the out-of-plane angular component with respect to the applied AC field that we shall estimate later.

A fundamental matrix solution of the system (70) and its inverse are given as

$$\mathbf{U}(t) = \begin{bmatrix} \omega_1 e^{\lambda_1 t} & 0 & \omega_3 e^{\lambda_3 t} \\ 0 & \Theta(t) & 0 \\ e^{\lambda_1 t} & 0 & e^{\lambda_3 t} \end{bmatrix}, \quad (87)$$

$$\mathbf{U}^{-1}(t) = \frac{1}{(\omega_1 - \omega_3)e^{(\lambda_1 + \lambda_3)t}\Theta(t)} \begin{bmatrix} \Theta(t)e^{\lambda_3 t} & 0 & -\omega_3\Theta(t)e^{\lambda_3 t} \\ 0 & e^{(\lambda_1 + \lambda_3)t}(\omega_1 - \omega_3) & 0 \\ -\Theta(t)e^{\lambda_1 t} & 0 & \omega_1\Theta(t)e^{\lambda_1 t} \end{bmatrix} \quad (88)$$

**Step 2.** Prior to solving the non-homogeneous system (70) we carry out an additional time-averaging, with the goal of simplifying the problem. Note that the first and second components of the vector field  $\mathbf{h}$ ,  $A_{12}\theta$  and  $A_{21}\phi$ , respectively, have the structure  $A_{12}(t) \sim \frac{L}{B}p(t)$ . We apply the averaging result that approximates solutions of a system of the form

$$\dot{\mathbf{x}} = \epsilon f(t, \mathbf{x}, \epsilon), \quad (89)$$

where  $0 < \epsilon$  is a small parameter, with those of

$$\dot{\mathbf{x}} = f_A(\mathbf{x}, 0). \quad (90)$$

Here  $f_A$  denotes the function that results from averaging the original  $f$  with respect to its explicit  $t$ -dependence, over an interval that, in our case, corresponds to a full period  $[0, 1]$ . The transformation from our original system (70) to one of the form (89) proceeds by a standard change of variable. The accuracy of the approximation relies on the smallness of  $\epsilon$  [33].

**Step 3.** Next, we solve the averaged simplified non-homogeneous system (70). First, we set up the variation of constant formula that now reads as

$$\mathbf{u}(t) = \mathbf{U}(t)[\mathbf{U}^{-1}(0)\mathbf{u}(0) + \int_0^t \mathbf{U}^{-1}(s) \begin{bmatrix} 0 \\ 0 \\ A_{32}(s)q(s) \end{bmatrix} ds]. \quad (91)$$

Details of the calculation of the terms in the previous equation are shown in the Supplemental Materials section. They lead to the solution

$$\begin{aligned} \phi(t) &= \frac{1}{\omega_1 - \omega_3} \{ (e^{\lambda_1 t} \omega_1 - e^{\lambda_3 t} \omega_3) \phi(0) \\ &+ \omega_1 \omega_3 (-e^{\lambda_1 t} + e^{\lambda_3 t}) q(0) \\ &+ \omega_1 \omega_3 \int_0^t A_{32}(s) \theta(s) (e^{\lambda_3(t-s)} - e^{-\lambda_1(t-s)}) ds \} \end{aligned} \quad (92)$$

$$\theta(t) = \Theta(t), \quad (93)$$

$$\begin{aligned} q(t) &= \frac{1}{\omega_1 - \omega_3} \{ (e^{\lambda_1 t} - e^{\lambda_3 t}) \phi(0) \\ &+ (-\omega_3 e^{\lambda_1 t} + \omega_1 e^{\lambda_3 t}) q(0) \end{aligned}$$

$$\begin{aligned} &+ C_2 \theta(0) \left( \frac{1}{\lambda_1^2 + 4\pi^2} [\lambda_1 e^{\lambda_1 t} - \lambda_1 \cos 2\pi t + 2\pi \sin 2\pi t] \right. \\ &\left. + \frac{C_1}{2(\lambda_1^2 + 16\pi^2)} [-\lambda_1 \sin 4\pi t - 4\pi \cos 4\pi t + 4\pi e^{\lambda_1 t}] \right), \end{aligned} \quad (94)$$

with as in (86), and

$$C_1 = \frac{M\sqrt{c_x}}{4B\pi\Delta_J}, \quad C_2 = \frac{2\lambda_\sigma Q_0 \Delta_1}{F\Delta_J} \sqrt{c_x}. \quad (95)$$

**Step 4.** We now summarise the neutral stability conditions that determine the speed and size range of the soliton-like distortions. These are of two types, involving the selection of special sets of initial data, and restrictions on the eigenvalues. First of all, from equation (86), we find two cases that lead to related but different instabilities:

$$C_0 = 0, \quad \lambda_3 = 0 \quad \text{and} \quad \lambda_3 - A_{22}^0 \neq 0, \quad \text{or} \quad (96)$$

$$\lambda_3 = A_{22}^0, \quad \text{and} \quad \lambda_3 = 0. \quad (97)$$

Note that the third condition in (96) guarantees that  $\Theta(0) \neq 0$ , needed for the invertibility of the fundamental matrix solution. Either set of relations also guarantee the preservation of the shape of  $\theta(t)$  with time and its phase shift with respect to the applied electric field. Finally, to preserve the shape of  $\phi$  and  $q$ , we additionally require

$$\lambda_1 = 0. \quad (98)$$

The observation in lemma (3.3) that  $A_{13}A_{31} = \frac{4L_2^2MQ_0\Delta_\sigma}{BF\Delta_J^2}c_x c_\xi$ , with  $L_2^2 = O(10^{-6})$ , together with  $\Delta_J \neq 0$ , allows us to obtain approximate forms of the vanishing conditions on the eigenvalues  $\lambda_1$  and  $\lambda_3$  in (76) as

$$A_{11} = A_{33} \quad \text{and} \quad A_{11} + A_{33} = 0. \quad (99)$$

The latter equation provides an expression of the tuxedo speed  $V$  as

$$\begin{aligned} 2V &= a_{11} + a_{33} \\ &= \frac{1}{\Delta_J} \left[ \frac{4}{B} (C\Delta_1\Delta_J + L_2^2 c_x c_\xi) + \frac{\Delta_\sigma}{F} (4G\Delta_J + Q_0M) \right]. \end{aligned} \quad (100)$$

The first equation in (99) evaluated at the parameter values of the problem, corresponds to the line

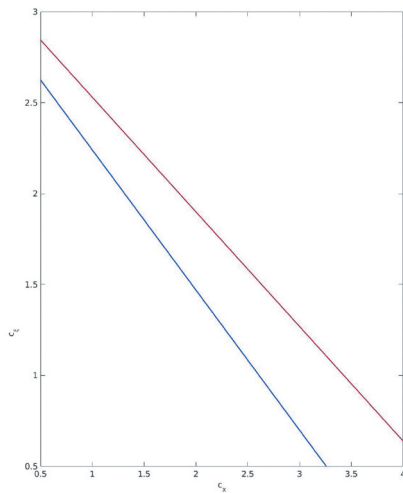
$$c_\xi + 0.7878c_x = 2.9740. \quad (101)$$

**Remark 5.** We find that, on the line (101),  $\Delta_\sigma = O(10^{-2})$  providing the estimate  $A_{13}A_{31} = O(L_i^2 \times 10^{-2})$  stated after Lemma (3.3). Furthermore,  $\Delta_1 \neq 0$ , for  $c_x \neq 0$ , holds for wave numbers on the line (101). The later justifies the initial layer argument stated in remark (2).

Moreover, evaluating  $V$  given by (100) on the curve (101) gives

$$V = \frac{1}{\Delta_J} \left[ \frac{\Delta_\sigma}{F} (4G\Delta_J + Q_0M) \right]. \quad (102)$$

The expression in (102) indicates that the sign of  $V$  is identical to that of  $\Delta_\sigma$ , provided  $\Delta_J > 0$ . We now evaluate  $V$  in (102) on the line (101) to get



$$V = \frac{0.0260 - 0.0127c_x}{F\Delta_J(c_x, c_\xi(c_x))} (4G\Delta_J + Q_0M), \quad (103)$$

where the  $\Delta_J$  expression in the denominator is evaluated on the line (101), where it satisfies  $\Delta_J > 0$  (see also figure 2). We observe that

$$\begin{aligned} \text{(i)} \quad &V > 0 \text{ for } c_x < 2.0472, \quad V = 0 \text{ at } c_x = 2.0472 \text{ and} \\ \text{(ii)} \quad &V < 0 \text{ for } 3.7751 \geq c_x > 2.0472, \end{aligned} \quad (104)$$

where the upper bound on  $c_x$  on the region of  $V < 0$  corresponds to the  $c_x$ -intercept of the line (101). The following lower bound on  $c_\xi$  follows from equation (101) and is associated with the  $c_x$ -interval indicated in (104), for the case  $V < 0$

$$0 \leq c_\xi \leq 1.3612 := c_\xi^{\max}. \quad (105)$$

We summarise the latter results on the graphs of Figure 2 and obtain estimates for the size of the disturbance. First of all, it is immediate to recover the wave numbers  $\rho_x$  and  $\rho_\xi$  from the quantities  $c_x$  and  $c_\xi$ , and subsequently derive estimates for the tuxedo size, that is, the width  $L_x$  and the length  $L_\xi$ :

$$\begin{aligned} |\rho_x| &= \frac{\sqrt{c_x}}{\pi\eta}, \quad |\rho_\xi| = \frac{\sqrt{c_\xi}}{\pi\eta}, \\ L_\xi &= |\rho_\xi|^{-1} \geq \frac{\pi\eta}{\sqrt{1.3621}} := L_\xi^{\min} = 2.6918\eta \\ \frac{\pi\eta}{\sqrt{2.0472}} = 2.1957\eta &= \geq L_x = |\rho_x|^{-1} \geq \frac{\pi\eta}{\sqrt{3.7751}} = 1.6169\eta. \end{aligned} \quad (106)$$

We note that the absolute value notation used in the expressions of the wave numbers is consistent with the assumptions (65). From the estimates in (106), we see that

$$L_{x,\text{phys}}^{\min} = 1.6169d \quad \text{and} \quad L_{\xi,\text{phys}}^{\min} = 2.6918d, \quad (107)$$

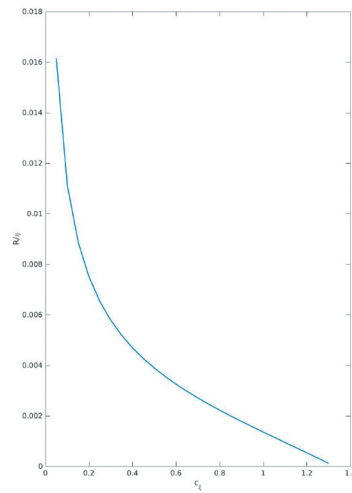


**Figure 2.** The top line on the figure on the left corresponds to the equation

where the latter quantities denote the dimensional sizes of the tuxedo on the units of the plate gap  $d$ . Comparing the length of the soliton package with that of the electrode plate  $L$ , we find that

$$L = 0.33 \times L_{\xi, \text{phys}}^{\min} \times 10^3. \quad (108)$$

From the point of view of the order of magnitude, the previous result agrees with the statement in [34] that the solitons travel on a plate several thousands of their own size.

We recall that the experimentally measured sizes, the width  $L_w$  and length  $L_l$ , of the soliton-like disturbances are reported as

$$L_w = 2d, \quad 20\mu\text{m} < L_l < 50\mu\text{m}. \quad (109)$$

Note that, for  $d = 8\mu\text{m}$ , the latter can be written as

$$2.5d\mu\text{m} < L_l < 6.25d\mu\text{m}, \quad (110)$$

showing an excellent agreement with the lower bound (107) of the soliton length predicted by our model.

In particular, the lower bound for the length corresponds to

$$c_l = 0.6806 = \frac{1}{2} c_{\xi}^{\max} \quad (111)$$

Next, we evaluate the phase-shift of the out-of-plane angle  $\theta$  in (86). For this, we calculate

$$\begin{aligned} & [2\pi \sin 2\pi t + (\lambda_3 - A_{22}^0) \cos 2\pi t] \\ &= 2\pi \left[ \sin 2\pi t + \frac{\lambda_3 - A_{22}^0}{2\pi} \cos 2\pi t \right] = 2\pi \sin(2\pi t - \alpha), \end{aligned} \quad (112)$$

with

$$\sin \alpha \approx \frac{4C}{2\pi B} = O(10^{-2}), \quad (113)$$

where we have applied the second relation in (96) as well as (64).

Finally, let us calculate the speed  $R$  of the soliton-like packages. First, note that

$$V = 2\pi R i \rho_{\xi} = -2\pi R \text{Im} \rho_{\xi} < 0 \Leftrightarrow R \text{Im} \rho_{\xi} > 0. \quad (114)$$

Hence, the  $c_x$ -region such that  $V < 0$  corresponds to  $R > 0$ , that is, the soliton disturbance travelling along the positive  $y$ -direction, provided  $\text{Im} \rho_x > 0$ . Furthermore, referring to the formula for the inverse Fourier transform, we find that  $\text{Im} \rho_{\xi} > 0$  corresponds to exponential *decay* along the positive  $y$ -direction. This, indeed, seems to correspond to the realistic physical setting, indicating that the perturbation has not yet reached, at time  $t > 0$ , locations such that  $y > > Rt$ .

Let us now compare the experimentally measured speed range  $R$  in (34) with the values displayed in the graph in figure 2. We first note that, for the aspect ratio  $\eta = 1.6 \times 10^{-3}$ , the experimental range previously referred to yields

$$0.0275 \leq \frac{R}{\eta} \leq 0.1400. \quad (115)$$

The discussion on the predicted soliton-like sizes in (106) suggests that the corresponding speeds, as shown in the graph of  $R - c_{\xi}$  in figure 2, fit towards the lower bound indicated in (115). If smaller solitons than the latter ones are to be taken into account, they would travel at speeds below than the lower bound in (115), up to an order of magnitude smaller. In conclusion, a decrease of the inter-plate gap  $d$  would bring a tighter agreement with the experimental findings.

We discard the solutions corresponding to  $V > 0$  in (101) that would yield disturbances with an exceedingly large horizontal size, vertically too short, and also with an incompatible growth rate.  $\Delta_j = 0$ . The bottom line on the same figure is the graph of equation (101), indicating that  $\Delta_j > 0$  on the points of the threshold line. The figure on the right represents the ratio,  $\frac{R}{\eta}$ , of the dimensionless speed of the soliton-like disturbance over the aspect ratio, as predicted by the model. The experimental measurements give  $\frac{R_{\min}}{\eta} = 0.0275$  and  $\frac{R_{\max}}{\eta} = 0.14$ .

## 4. Conclusion

In this article, we have developed a time-dependent model of a flexoelectric nematic liquid crystal that couples elastic, viscous, conducting, dielectric and flexoelectric effects. We use linear analysis to investigate the three-dimensional solitons observed when such a material is subject to an alternating electric field, within the appropriate range of intensity and frequency. The work focuses on finding the instability threshold of the uniformly aligned nematic, and yields estimates on the size, phase-shift and speed of the soliton-like package. The length and speed of the soliton predicted by the model fall towards the lower range of the experimentally measured ones. The work presented here is the first part of the three article set devoted to the study of the physical solitons reported in [34]. A forthcoming nonlinear analysis aims at correcting the lower predictions of the present linear model, which will also address finer aspects of the soliton shape, such as the size of the



head versus the tail. Finally, the third article will focus on the well posedness of flexoelectric nematic models that present additional nontrivial challenges due to the higher order gradient of the theory, compared with standard nematic.

## Acknowledgments

The authors want to express their gratitude to Professor Oleg Lavrentovich for the many discussions and the sharing of experimental results, and to Professor Dmitry Golovaty for his helpful comments.

## Disclosure statement

No potential conflict of interest was reported by the author(s).

## Funding

The authors gratefully acknowledge the support of the National Science Foundation through the grant DMS-DMREF 1729589.

## References

- [1] Li B-X, Borshch V, Xiao R-L, et al. Electrically driven three-dimensional solitary waves as director bullets in nematic liquid crystals. *Nat Commun.* 2018;9:1–10. .
- [2] Buka A, Eber N. Flexoelectricity in liquid crystals: theory, experiments and applications. World Scientific; 2013.
- [3] Buka A, Éber N, Pesch W, et al. Convective patterns in liquid crystals driven by electric field. In: Byrnes, J., and Ostheimer, G. editor. *Advances in sensing with security applications*. Dordrecht: Springer; 2006. p. 55–82.
- [4] de Gennes PG, Prost J, editors. *The physics of liquid crystals*. New York: Oxford University Press; 1993.
- [5] Fredericksz V, Zolina V. Forces causing the orientation of an anisotropic liquid. *Trans Faraday Soc.* 1933;29:919–930.
- [6] Zocher H. The effect of a magnetic field on the nematic state. *Trans Faraday Soc.* 1933;29(140):945–957.
- [7] Bénard H. Les tourbillons cellulaires dans une nappe liquide. *Rev Gen Sci Pures Appl.* 1900;11:1261–1271.
- [8] Rayleigh L. Lix. on convection currents in a horizontal layer of fluid, when the higher temperature is on the under side. London, Edinburgh, Dublin *Philos Mag J Sci.* 1916;32(192):529–546.
- [9] Koschmieder EL. Bénard cells and Taylor vortices. Cambridge, England: Cambridge University Press; 1993.
- [10] Williams R. Domains in liquid crystals. *J Chem Phys.* 1963;39(2):384–388.
- [11] Kapustin AP, Larinova L. On the behavior of anisotropic liquids in electric fields. *Kristallografiya.* 1964;9(2):297–300.
- [12] Carr EF. Influence of electric fields on the molecular alignment in the liquid crystal p(anisalamino)-phenyl acetate. *Mol Cryst Liq Cryst.* 1969;7(1):253–268.
- [13] Dubois-Violette E, de Gennes PG, Parodi O. Hydrodynamic instabilities of nematic liquid crystals under a. c. electric fields. *J Phys France.* 1971;32(4):305–317.
- [14] Helfrich W. Conduction-induced alignment of nematic liquid crystals: basic model and stability considerations. *J Chem Phys.* 1969;51(9):4092–4105.
- [15] Dubois-Violette E, De Gennes PG, Parodi O. Hydrodynamic instabilities of nematic liquid crystals under ac electric fields. *J Phys.* 1971;32(4):305–317.
- [16] Kramer L, Pesch W. Convection instabilities in nematic liquid crystals. *Annu Rev Fluid Mech.* 1995;27(1):515–539.
- [17] Wiant D, Gleeson JT, Eber N, et al. Nonstandard electroconvection in a bent-core nematic liquid crystal. *Phys Rev E.* 2005;72(4):041712.
- [18] Shiomi M, Choi E-J, Huh J-H. Prewavy instability-originated dielectric chevrons of electroconvection in nematic liquid crystals. *Phys Rev E.* 2020;102(4):042704.
- [19] Huh J-H, Miyagawa N. Reentrant prewavy instability in competition between rising and twist modes in ac field-driven electroconvection. *Phys Rev E.* 2021;103(6):062701.
- [20] Meyer RB. Piezoelectric effects in liquid crystals. *Phys Rev Lett.* 1969;22(18):918.
- [21] Krekhov A, Pesch W, Buka A. Flexoelectricity and pattern formation in nematic liquid crystals. *Phys Rev E.* 2011;83(5):051706.
- [22] Zabusky NJ, Kruskal MD. Interaction of "solitons" in a collisionless plasma and the recurrence of initial states. *Phys Rev Lett.* 1965;15(6):240.
- [23] Tao T. Why are solitons stable? *Bull Am Math Soc.* 2009;46(1):1–33.
- [24] Reimbert CG, Minzoni AA, Smyth NF, et al. Large amplitude nematicon propagation in a liquid crystal with local response. *J Opt Soc Am B.* 2006 Dec;23(12):2551–2558.
- [25] Borgna JP, Panayotaros P, Rial D, et al. Optical solitons in nematic liquid crystals: model with saturation effects. *Nonlinearity.* 2018 mar;31(4):1535–1559.
- [26] Earls A. Flexoelectricity and three-dimensional solitons in nematic liquid crystals. PhD thesis, University of Minnesota, December 2019.
- [27] Garbovskiy Y. Evaluating the concentration of ions in liquid crystal cells: hidden factors and useful techniques. *Multidiscip Digital Publ Inst Proc.* 2021;62:10.
- [28] Sonnet AM, Virga EG. Dynamics of dissipative ordered fluids. *Phys Rev E.* 2001;64:031705.
- [29] Castles F, Green SC, Gardiner DJ, et al. Flexoelectric coefficient measurements in the nematic liquid crystal phase of 5cb. *AIP Adv.* 2012;2(2):022137.
- [30] Cheung DL, Clark SJ, Wilson MR. Calculation of flexoelectric coefficients for a nematic liquid crystal by atomistic simulation. *J Chem Phys.* 2004;121(18):9131–9139.
- [31] O'malley RE. Singular perturbation methods for ordinary differential equations. Vol. 89. New York, NY: Springer; 1991.
- [32] Hale JK. Ordinary differential equations. Vol. 21. 2d. Huntington (N.Y.): R. E. Krieger Pub. Co; 1980. Pure and applied Mathematics
- [33] Sanders JA, Verhulst F, Murdock J. Averaging methods in nonlinear dynamical systems. Vol. 59. New York, NY: Springer; 2007.
- [34] Borshch V, Lavrentovich O. Localized moving soliton-like distortions of the director of a liquid crystal. Kent, Ohio: Kent State University, private communication; 2018.